Sequential tunneling transport characteristics of GaN/AlGaN coupled-quantum-well structures

Faisal Sudradjat, Wei Zhang, Kristina Driscoll, Yitao Liao, Anirban Bhattacharyya et al.

Additional information on J. Appl. Phys.

Sequential tunneling transport characteristics of GaN/AlGaN coupled-quantum-well structures

Faisal Sudradjat,[1] Wei Zhang,[1] Kristina Driscoll,[1] Yitao Liao,[1] Anirban Bhattacharyya,[1] Christos Thomidis,[1] Lin Zhou,[2] David J. Smith,[2] Theodore D. Moustakas,[1] and Roberto Paiella[1,a)]

[1]*Department of Electrical and Computer Engineering and Photonics Center, Boston University, 8 Saint Mary's Street, Boston, Massachusetts 02215, USA*
[2]*Department of Physics, Arizona State University, Tempe, Arizona 85287, USA*

Vertical electronic transport in periodic GaN/AlGaN multiple-quantum-well structures grown on free-standing GaN substrates is investigated. Highly nonlinear current-voltage characteristics are measured, displaying a clear transition from a high-resistance state near zero applied bias to a low-resistance state as the voltage is increased. The measurement results, including their temperature dependence and the variations in turn-on voltage with subband structure and bias polarity are in full agreement with a picture of sequential tunneling through the ground-state subbands of adjacent coupled quantum wells. Scattering-assisted tunneling due to interface roughness or structural defects appears to be the dominant transport mechanism. The potential role of photon-assisted tunneling is also investigated. © *2010 American Institute of Physics*. [doi:10.1063/1.3511334]

I. INTRODUCTION

As the materials and device technology of III-nitride semiconductors continues to make progress, new applications are constantly emerging in electronics and optoelectronics. As an important example, substantial research efforts are currently being devoted to the study of novel device functionalities based on intersubband transitions in these materials.[1–11] These activities are motivated by the large conduction-band offsets of GaN/Al(Ga)N quantum wells (QWs), which allow extension of the intersubband transition wavelength to the near-infrared spectral region, and by their large optical phonon energies, which are favorable in the context of terahertz optoelectronics.[2,4,10] Recent milestones include the demonstration of intersubband optically pumped light emission,[7,11] all-optical switching,[5,6] electro-optic modulation,[8] and photodetection in multiple-QW and quantum cascade structures.[3,9] On the other hand, the study of tunneling transport in nitride QWs, which is a key feature of several intersubband devices including quantum cascade lasers,[12] has so far been limited.

The main challenge in this context is provided by the relatively large densities of dislocations and other structural defects that are typically found in nitride semiconductors, especially when grown on highly lattice-mismatched sapphire substrates. In general, such defects can act as strong scattering centers, as well as parallel current paths partially shorting out the QWs in high-resistance vertical-transport devices. Recently, negative differential resistance has been observed at room temperature in GaN/Al(Ga)N double-barrier structures and attributed to resonant tunneling.[13–16] However, this behavior was found to slowly degrade after each measurement (possibly due to activated filling of trap states) and

to be accompanied by a hysteresis that could not be explained using simple models. Here, we consider a different situation where electrons traverse thick periodic structures based on triple-QW repeat units, similar in principle to typical quantum cascade active regions. Stable and highly nonlinear vertical transport characteristics are observed, fully consistent with a picture of scattering-assisted sequential tunneling. Interface roughness, which can provide a substantial change in the electronic in-plane wave vector, is identified as the likely dominant scattering mechanism. These results underscore the feasibility as well as present limitations of complex nitride devices based on tunneling transport.

II. SAMPLE DESIGN AND GROWTH

The samples used in this study were grown by rf plasma-assisted molecular beam epitaxy on commercially available 300-μm-thick free-standing GaN substrates, with typical threading dislocation densities of $1-2 \times 10^7$ cm^{-2}. Two different structures (labeled A and B in the following) were investigated, consisting of 20 and 30 repetitions, respectively, of two different GaN/Al$_{0.15}$Ga$_{0.85}$N triple-QW periods. The individual layers in each repeat unit have nominal thicknesses of **12**, 13, **7**, 9, **9**, and 15 monolayers (MLs) in structure A, and **9**, 18, **4**, 9, **10**, and 19 MLs in structure B, where the bold typeface denotes the Al$_{0.15}$Ga$_{0.85}$N barriers and 1 ML ≈ 2.6 Å. The underlined thicknesses indicate wells that are *n*-doped with Si to a level of approximately 5×10^{10} cm^{-2}, while all other QW layers are nominally intrinsic. Before growth, the substrates were prepared with the planarization technique developed in Ref. 17, in order to eliminate residual scratches due to the mechanical polishing used in their fabrication. Thick GaN and Al$_{0.05}$Ga$_{0.95}$N films doped *n*-type to the level of 7×10^{18} cm^{-3} were then deposited in structures A and B, respectively, followed by the
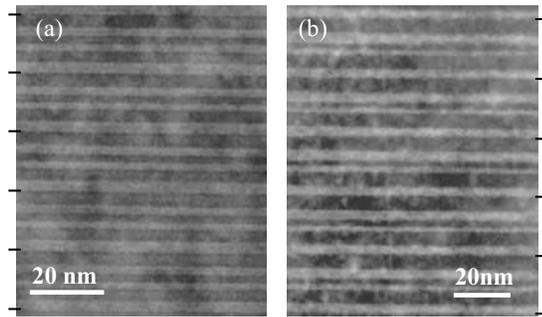
a)Electronic mail: rpaiella@bu.edu.

FIG. 1. Cross-sectional TEM images of the periodic multiple-QW structures A (a) and B (b) studied in this work. The horizontal lines on either side of each image indicate the boundaries between adjacent repeat units. The darker and lighter regions correspond to the GaN and $Al_{0.15}Ga_{0.85}N$ layers, respectively.

multiple-QW region, and finally by a 200-nm cap layer of the same composition with Si doping density of $1-2 \times 10^{18}$ cm^{-3}. Thus, both the bottom and the top contact layers are doped to a degenerate level, which ensures good electrical conductivity over the entire temperature range investigated.[18] At the same time, the separation between the top of the barriers and the Fermi level in the contact layers is sufficiently large that carrier spill-over into the continuum of unbound states over the QWs can be safely neglected, even at room temperature.

The QW layer thicknesses were examined using a 400-keV JEM-4000EX transmission electron microscope (TEM). Cross-sectional TEM images of a few adjacent QWs of structures A and B are shown in Figs. 1(a) and 1(b), respectively, where the darker (lighter) regions correspond to the GaN ($Al_{0.15}Ga_{0.85}N$) layers, and the short horizontal lines drawn on either side of each image indicate the boundaries between consecutive repeat units. As shown in these figures, the individual layer thicknesses are in good agreement with the nominal values, with typical period-to-period and in-plane variations of only about one ML. The epilayer interfaces also appear to be relatively abrupt and well defined. At the same time, lower magnification images reveal the presence of dislocations passing through the multiple-QW layers, as typically observed in this materials system.

Figures 2 and 3 show the conduction-band lineups of two repeat units of structures A and B, respectively, under different bias conditions. The horizontal axes in these plots indicate position along the growth direction, increasing toward the cap layer from left to right. The squared envelope functions of the relevant subbands are also shown referenced to their respective energy levels. These quantities were calculated using a Schrödinger equation solver that includes the characteristic pyro- and piezoelectric fields of nitride heterostructures, with all the relevant material parameters taken from Ref. 19. The intrinsic electric fields were computed using periodic boundary conditions, i.e., by requiring that in the absence of any external bias the voltage across each repeat unit is zero. This assumption is appropriate to the description of thick periodic structures consisting of many repeat units, especially when the well and barrier compositions are close to those of the template and cap layer, as in the present samples.[20]
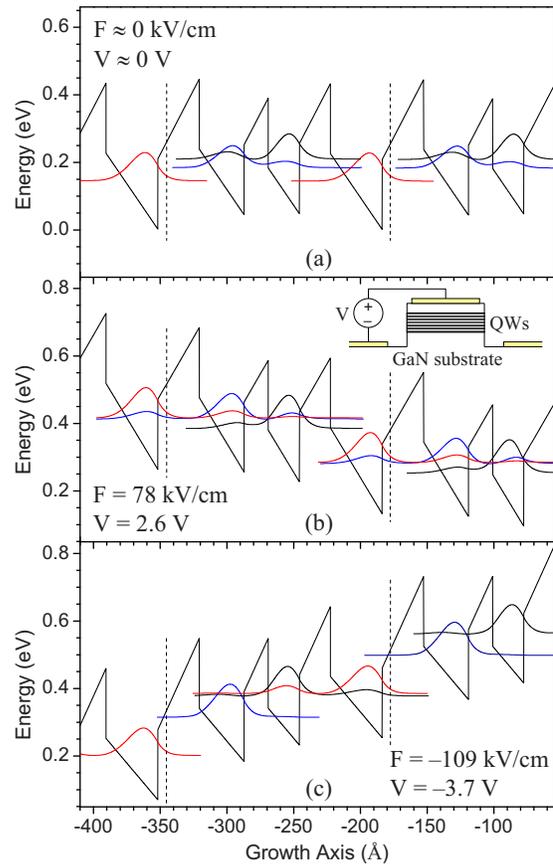

FIG. 2. (Color online) Conduction-band lineup of two repeat units of structure A and squared envelope functions of the ground-state subbands, under different bias conditions: (a) near zero applied voltage V; (b) for V =2.6 V, as required for efficient tunneling transport in the forward direction; and (c) for V=−3.7 V, as required for efficient tunneling transport in the reverse direction. The vertical dashed lines in each plot indicate the boundaries between adjacent repeat units. The inset of Fig. 2(b) shows a schematic cross-sectional view of a processed device, and defines the voltage polarity convention used in this work.

The expected tunneling transport characteristics of the two structures under study can be inferred from the plots of Figs. 2 and 3. Considering structure A first, its conduction-band diagram in the case of near zero applied bias is shown in Fig. 2(a). Under these conditions, the electrons supplied by the Si donors in each repeat unit mostly reside in the ground-state subband of the widest well (i.e., the 15-ML-thick, right-most well of each triple-QW period in the figure). These subbands are energetically separated from the ground states of the neighboring wells by relatively large amounts (about 40 and 65 meV for the wells immediately above and immediately below, respectively). As a result, the entire structure is in a state of relatively high resistance, especially at low temperature. As the bias is increased in either direction, the populated subbands become energetically aligned with the ground states of the adjacent wells downstream. Consequently, vertical transport by sequential tunneling (either resonant or scattering-assisted) becomes allowed and the differential resistance is lowered.

Due to the asymmetric nature of this multiple-QW structure, the voltage drop required to achieve a suitable subband alignment for efficient electronic transport is different depending on whether it is applied from top to bottom or vice
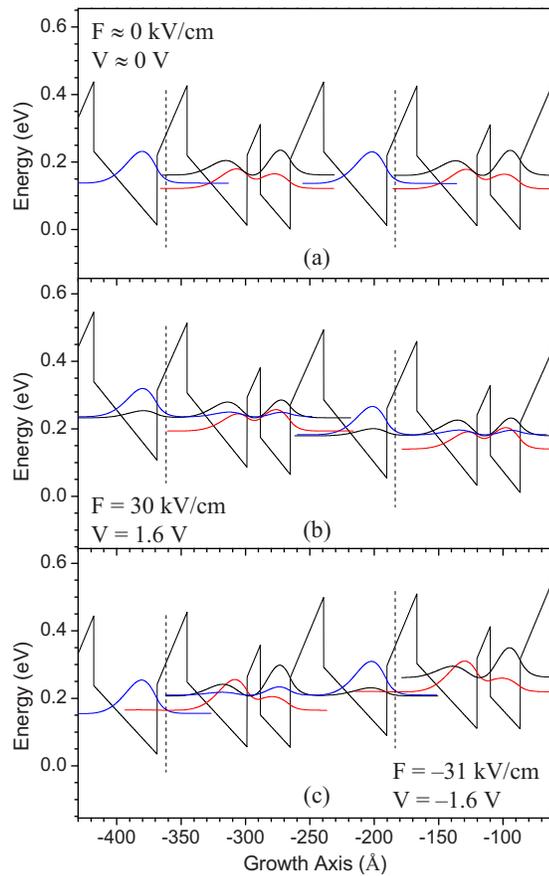
FIG. 3. (Color online) Conduction-band lineup of two repeat units of structure B and squared envelope functions of the ground-state subbands, under different bias conditions: (a) near zero applied voltage V; (b) for V =1.6 V, as required for efficient tunneling transport in the forward direction; and (c) for V=−1.6 V, as required for efficient tunneling transport in the reverse direction. The vertical dashed lines in each plot indicate the boundaries between adjacent repeat units.

versa. In particular, as shown in Fig. 2(b), the ground-state subband of each 15-ML well is brought into alignment with that of its overlaying well by an external electric field F of 78 kV/cm, corresponding to a voltage V of about 2.6 V across the 20 repeat units. On the other hand, as shown in Fig. 2(c), a larger electric field of 109 kV/cm (corresponding to a voltage of 3.7 V) is required to achieve ground-state subband alignment between each 15-ML well and its adjacent well below. Therefore, the expected transition to a low-resistance state should occur at a larger value of the applied voltage in the case of "negative" or "reverse" bias polarity (i.e., in the presence of a voltage drop from the template to the cap layer).

Similarly nonlinear electrical characteristics are also expected in the case of structure B. An important difference, however, is the fact that near zero bias this structure features a relatively symmetric subband arrangement, as shown in Fig. 3(a). Specifically, the lowest-energy subband of each repeat unit here is fully delocalized across a pair of coupled QWs, whose two neighboring wells (immediately above and immediately below) are identical to each other. As a result, comparable turn-on voltages are expected in the forward- and reverse-bias directions. In fact, as shown in Figs. 3(b) and 3(c), a suitable subband alignment for electronic trans-

port is obtained with forward and reverse applied electric fields of 30 kV/cm and 31 kV/cm, respectively. The corresponding voltage across the 30 periods of this structure is approximately 1.6 V in each case. It should also be noted that this value is significantly smaller than the forward and reverse turn-on voltages of sample A, which is also a consequence of their different subband structures.

III. RESULTS AND DISCUSSION

To verify these predictions experimentally, 450 ×400 μm^2 mesa-structure devices were fabricated by inductively coupled plasma etching through the multiple-QW layer using a chlorine-based chemistry. Metal contacts consisting of Ti/Al/Ti/Au layers were then deposited by electron-beam evaporation and liftoff on top of and around each mesa. These electrodes were characterized using a standard transmission line method in a two-point probe configuration on the same wafers, and found to be Ohmic with specific contact resistance on the order of 10^{-4} Ω cm^2, which is small enough to have negligible effect on the measured electrical characteristics. A schematic cross-sectional image of a processed device is shown in the inset of Fig. 2(b). After metallization, the samples were annealed in a forming gas environment in order to passivate possible defects on the mesa sidewalls that could provide parallel current paths. The devices were then soldered onto a copper block, wire-bonded, and finally mounted on the cold finger of a suitably wired continuous-flow liquid-helium cryostat.

Exemplary current-voltage (I-V) characteristics measured from a device based on structure A using positive (i.e., top to bottom) and negative voltage pulses are shown in Figs. 4(a) and 4(b), respectively. The different curves in each plot correspond to heat-sink temperatures of 20, 100, 200, and 280 K in order of increasing current for fixed voltage. The bias pulse width and repetition rate are 200 ns and 20 kHz, respectively, corresponding to a duty cycle of 0.4%. It should be noted that the same results were also obtained for a wide range of values of pulse width and duty cycle up to an order of magnitude higher, indicating that the observed electrical characteristics are not affected by device heating during each scan. Furthermore, these traces were found to be stable and fully reproducible throughout many repeated measurements. The device low-temperature differential resistance R_{diff} =dV/dI, obtained from the measured I-V traces at 20 K, is plotted versus voltage in Fig. 4(c), where the solid and dotted lines correspond to negative and positive bias, respectively.[21] Finally, Fig. 5 is equivalent to Fig. 4 except that it shows data measured with a device based on structure B.

As expected, the I-V curves of both devices are strongly nonlinear and clearly display a transition from a high-resistance state near zero applied bias to a low-resistance state as the voltage is increased. In the case of sample A, this transition occurs at significantly higher voltage when pulses of negative polarity are used, as in Fig. 4(b), compared to the case of positive pulses shown in Fig. 4(a). In the case of sample B, the forward and reverse I-V curves reach the low-resistance regime at comparable values of the applied bias. Furthermore, these values are substantially smaller than the
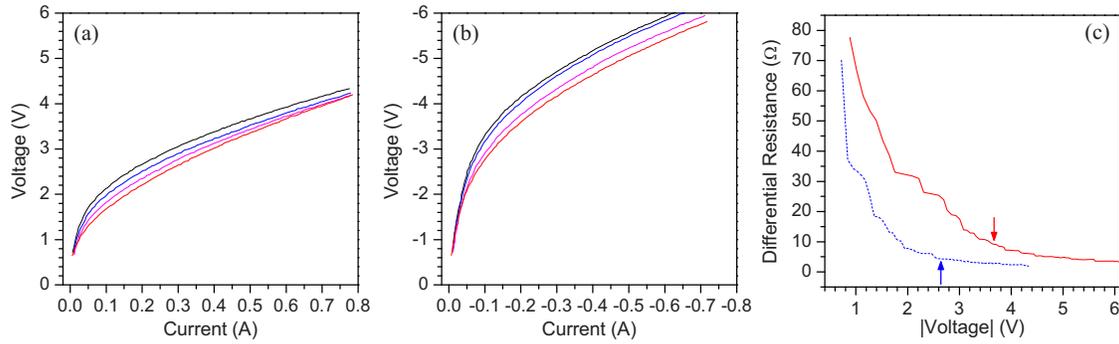
FIG. 4. (Color online) I-V characteristics measured from a device based on structure A at different heat-sink temperatures, using positive (a) and negative (b) voltage pulses. The four curves in each plot correspond to a temperature of 20, 100, 200, and 280 K in order of increasing current for fixed voltage. (c) Differential resistance obtained from the measured I-V curves at 20 K under reverse (solid line) and forward (dotted line) bias, plotted as a function of voltage. The arrow next to each trace denotes the corresponding theoretical turn-on voltage.

corresponding turn-on voltages of sample A. All of these observations are in full agreement with the aforementioned theoretical expectations based on the simulation results of Figs. 2 and 3. For a more detailed comparison, the calculated forward and reverse turn-on voltages are also shown in Figs. 4(c) and 5(c) by the vertical arrows next to the corresponding traces. In each case, the differential resistance rapidly decreases with increasing voltage below the value denoted by the arrow, and then remains relatively constant for larger voltages. The temperature dependence of these measured I-V curves is also consistent with tunneling transport. Specifically, as the temperature is increased the current turn-on becomes more gradual and shifts to lower values of the applied bias, due to the thermal broadening of the electronic distribution in the initially occupied subbands.

These results, therefore, indicate the feasibility of complex GaN/AlGaN multiple-QW structures where vertical transport involves efficient sequential tunneling. It should be noted that parallel current paths due to dislocations and other structural defects may still exist in the samples under study, and could also contribute to their transport properties. However, the strong correlation observed between the measured I-V characteristics and the calculated subband structures provides compelling evidence that the majority of injected electrons indeed traverse the samples via tunneling through the QW bound states.

We also note that no signatures of negative differential resistance are observed in the data of Figs. 4 and 5. In fact, in general the measured differential resistances remain relatively constant as the bias is increased above the turn-on value, indicating that scattering plays a major role in the measured transport properties. Thus, efficient elastic tunneling can occur even when the initial subband is at higher energy than the final one, with the required change in in-plane wave vector provided by the scattering mechanism involved. A likely candidate is scattering by interface roughness, which features a weak dependence on intersubband energy separation over a wide range.[22] Additional mechanisms that may also be involved include scattering by compositional inhomogeneities and structural defects, as well as inelastic tunneling via LO-phonon emission in the case of structure A (where some of the adjacent ground-state subbands have sufficiently large energy separation). As an exception to the general behavior just described, a clear increase in differential resistance with increasing voltage above turn-on is observed in the case of structure B under forward bias and low temperature [see Figs. 5(a) and 5(c)]. This indicates sufficiently large misalignment of the relevant subbands and/or spatial separation of the relevant envelope functions to substantially reduce the efficiency of the underlying scattering processes.

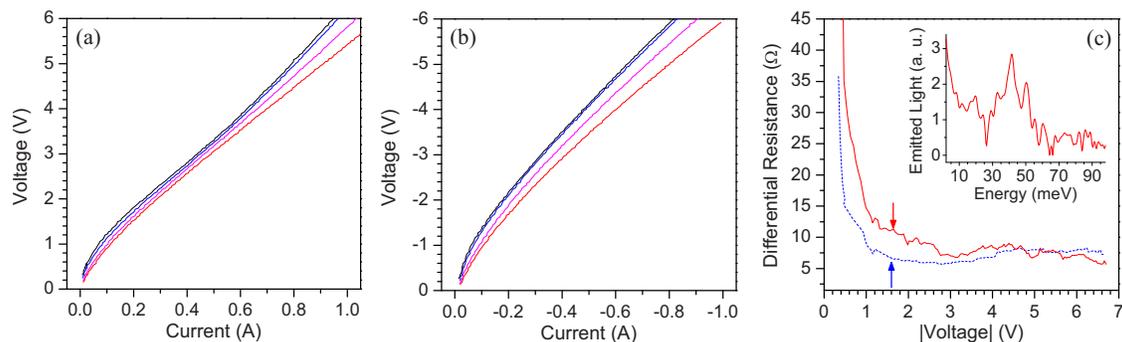Finally, we address the question of whether the measured

FIG. 5. (Color online) I-V characteristics measured from a device based on structure B at different heat-sink temperatures, using positive (a) and negative (b) voltage pulses. The four curves in each plot correspond to a temperature of 20, 100, 200, and 280 K in order of increasing current for fixed voltage. (c) Differential resistance obtained from the measured I-V curves at 20 K under reverse (solid line) and forward (dotted line) bias, plotted as a function of voltage. The arrow next to each trace denotes the corresponding theoretical turn-on voltage. The inset shows a far-infrared electroluminescence spectrum measured from the same device.

electrical characteristics may also have a contribution from photon-assisted tunneling (i.e., interwell intersubband emission), which provides an obvious device application for the types of structures considered in this work. To investigate this question, far-infrared electroluminescence measurements were carried out via step-scan lock-in detection with a Fourier transform infrared spectrometer equipped with a Si bolometer. Light emission in the expected wavelength range was observed from several devices based on both structures, with a grating in the top metal contact used for normal-incidence outcoupling of in-plane emitted radiation. A representative spectrum, measured with a sample based on structure B under reverse bias at 20 K, is shown in the inset of Fig. 5(c), where a broad peak superimposed on a longer-wavelength shoulder is clearly resolved. While these results are promising, the measured spectra are generally too weak and broad to be unambiguously attributed to intersubband transitions as opposed to heating of the electron gas or other mechanisms. Further improvements in material quality and perhaps design strategy will therefore likely be required to make further progress in this direction.

IV. CONCLUSIONS

In summary, we have investigated the vertical transport properties of two GaN/AlGaN periodic QW structures. Nonlinear I-V characteristics were consistently measured, featuring a clear transition from a high-resistance state near zero applied bias to a low-resistance state as the voltage is increased. The experimental data, including their temperature dependence and the variations in turn-on voltage with subband structure and bias polarity, are in full agreement with a picture of scattering-assisted tunneling through the QW bound states. Interface roughness is likely to be the dominant scattering mechanism, as it can provide the large in-plane wave vector change that is required for elastic tunneling between subbands of different energy minima. From a device design perspective, these observations indicate that selective electron injection via tunneling in these QWs will need to rely on careful engineering of the relevant envelope-function overlaps. Far-infrared light emission was also observed with the same samples indicating the possibility of photon-assisted tunneling, although the measured spectra are too weak and broad for a conclusive identification of the emission mechanism. While further materials advances may be needed in the latter respect, the feasibility of tunneling transport presented here is promising for future device applications of complex nitride quantum structures.

[1] C. Gmachl, H. M. Ng, S.-N. G. Chu, and A. Y. Cho, Appl. Phys. Lett. **77**, 3722 (2000).
[2] V. D. Jovanović, D. Indjin, Z. Ikonić, and P. Harrison, Appl. Phys. Lett. **84**, 2995 (2004).
[3] E. Baumann, F. R. Giorgetta, D. Hofstetter, H. Lu, X. Chen, W. J. Schaff, L. F. Eastman, S. Golka, W. Schrenk, and G. Strasser, Appl. Phys. Lett. **87**, 191102 (2005).
[4] G. Sun, R. A. Soref, and J. B. Khurgin, Superlattices Microstruct. **37**, 107 (2005).
[5] N. Iizuka, K. Kaneko, and N. Suzuki, IEEE J. Quantum Electron. **42**, 765 (2006).
[6] Y. Li, A. Bhattacharyya, C. Thomidis, T. D. Moustakas, and R. Paiella, Opt. Express **15**, 17922 (2007).
[7] L. Nevou, M. Tchernycheva, F. H. Julien, F. Guillot, and E. Monroy, Appl. Phys. Lett. **90**, 121106 (2007).
[8] L. Nevou, N. Kheirodin, M. Tchernycheva, L. Meignien, P. Crozat, A. Lupu, E. Warde, F. H. Julien, G. Pozzovivo, S. Golka, G. Strasser, F. Guillot, E. Monroy, T. Remmele, and M. Albrecht, Appl. Phys. Lett. **90**, 223511 (2007).
[9] A. Vardi, G. Bahir, F. Guillot, C. Bougerol, E. Monroy, S. E. Schacham, M. Tchernycheva, and F. H. Julien, Appl. Phys. Lett. **92**, 011112 (2008).
[10] E. Bellotti, K. Driscoll, T. D. Moustakas, and R. Paiella, Appl. Phys. Lett. **92**, 101112 (2008).
[11] K. Driscoll, Y. Liao, A. Bhattacharyya, L. Zhou, D. J. Smith, T. D. Moustakas, and R. Paiella, Appl. Phys. Lett. **94**, 081120 (2009).
[12] C. Sirtori, F. Capasso, J. Faist, A. L. Hutchinson, D. L. Sivco, and A. Y. Cho, IEEE J. Quantum Electron. **34**, 1722 (1998).
[13] A. Kikuchi, R. Bannai, K. Kishino, C.-M. Lee, and J.-I. Chyi, Appl. Phys. Lett. **81**, 1729 (2002).
[14] A. E. Belyaev, O. Makarovsky, D. J. Walker, L. Eaves, C. T. Foxon, S. V. Novikov, L. X. Zhao, R. I. Dykeman, S. V. Danylyuk, S. A. Vitusevich, M. J. Kappers, J. S. Barnard, and C. J. Humphreys, Physica E (Amsterdam) **21**, 752 (2004).
[15] S. Golka, C. Pflügl, W. Schrenk, G. Strasser, C. Skierbiszewski, M. Siekacz, I. Grzegory, and S. Porowski, Appl. Phys. Lett. **88**, 172106 (2006).
[16] C. Bayram, Z. Vashaey, and M. Razeghi, Appl. Phys. Lett. **96**, 042103 (2010).
[17] A. D. Williams and T. D. Moustakas, *Advances in III-V Nitride Semiconductor Materials and Devices*, MRS Symposia Proceedings No. 892 (Materials Research Society, Pittsburgh, 2006), p. 363.
[18] R. J. Molnar, T. Lei, and T. D. Moustakas, Appl. Phys. Lett. **62**, 72 (1993).
[19] I. Vurgaftman and J. R. Meyer, J. Appl. Phys. **94**, 3675 (2003).
[20] S. Gunna, F. Bertazzi, R. Paiella, and E. Bellotti, in *Nitride Semiconductor Devices: Principles and Simulations*, edited by J. Piprek (Wiley, New York, 2007), Chap. 6.
[21] The electrical pulse generator used in these measurements has a finite minimum output power, and as a result the I-V traces could not be measured all the way down to zero voltage. The differential resistance near V=0 was estimated with an ohmmeter (supplying a small current of 1 mA) and found to be larger than 500 Ω at 20 K.
[22] T. Unuma, M. Yoshita, T. Noda, H. Sakaki, and H. Akiyama, J. Appl. Phys. **93**, 1586 (2003).